Journal of Quantitative Spectroscopy & Radiative Transfer ∎ (∎∎∎∎) ∎∎∎–∎∎∎

Contents lists available at ScienceDirect

Journal of Quantitative Spectroscopy & Radiative Transfer

journal homepage: www.elsevier.com/locate/jqsrt

Optimized approach to retrieve information on atmospheric carbonyl sulfide (OCS) above the Jungfraujoch station and change in its abundance since 1995

Bernard Lejeune [a,*], Emmanuel Mahieu [a], Martin K. Vollmer [b], Stefan Reimann [b], Peter F. Bernath [c,d], Christopher D. Boone [d], Kaley A. Walker [e], Christian Servais [a]

[a] Institute of Astrophysics and Geophysics of the University of Liège, Liège, Belgium
[b] EMPA, Laboratory for Air Pollution/Environmental Technology, Duebendorf, Switzerland
[c] Department of Chemistry and Biochemistry, Old Dominion University, Norfolk, Virginia
[d] Department of Chemistry, University of Waterloo, Ontario, Canada
[e] Department of Physics, University of Toronto, Ontario, Canada

ARTICLE INFO

Article history:
Received 14 February 2016
Received in revised form
1 June 2016
Accepted 1 June 2016

Keywords:
OCS
FTIR spectroscopy
Jungfraujoch
ACE-FTS
GCMS

ABSTRACT

In this paper, we present an optimized retrieval strategy for carbonyl sulfide (OCS), using Fourier transform infrared (FTIR) solar observations made at the high-altitude Jungfraujoch station in the Swiss Alps. More than 200 lines of the ν_3 fundamental band of OCS have been systematically evaluated and we selected 4 microwindows on the basis of objective criteria minimizing the effect of interferences, mainly by solar features, carbon dioxide and water vapor absorption lines, while maximizing the information content. Implementation of this new retrieval strategy provided an extended time series of the OCS abundance spanning the 1995–2015 time period, for the study of the long-term trend and seasonal variation of OCS in the free troposphere and stratosphere.

Three distinct periods characterize the evolution of the tropospheric partial columns: a first decreasing period (1995–2002), an intermediate increasing period (2002–2008), and the more recent period (2008–2015) which shows no significant trend. Our FTIR tropospheric and stratospheric time series are compared with new in situ gas chromatography mass spectrometry (GCMS) measurements performed by Empa (Laboratory for Air Pollution/Environmental Technology) at the Jungfraujoch since 2008, and with space-borne solar occultation observations by the ACE-FTS instrument on-board the SCISAT satellite, respectively, and they show good agreement. The OCS signal recorded above Jungfraujoch appears to be closely related to anthropogenic sulfur emissions.

1. Introduction

With a global average tropospheric mixing ratio of about 500 pptv (parts per trillion by volume) [1] and an atmospheric lifetime of about 2.5 years [2], OCS is the most abundant sulfur-containing compound in the free troposphere. The main sources of atmospheric OCS are [3]: the atmospheric oxidation of dimethyl sulfide (DMS) from marine plankton, oxidation of carbon disulfide (CS_2) from industrial and marine natural origin, and the gas exchange of OCS between the oceans and the atmosphere. The main sinks are uptake by land plants, uptake by oxic soils, and atmospheric oxidation by hydroxyl radicals.

OCS is an atmospheric trace gas which is gaining increasing attention from the scientific community. First considered for its role in the Earth's radiation balance as a contributor to

* Corresponding author.
E-mail address: bernard.lejeune@ulg.ac.be (B. Lejeune).

http://dx.doi.org/10.1016/j.jqsrt.2016.06.001
0022-4073/

the non-volcanic background sulfate layer in the stratosphere [4], it has been suggested more recently that atmospheric OCS measurements have the potential to become an atmospheric tracer of Gross Primary Production (GPP) and thus it holds great promise for studies of carbon cycle processes [2]. As a result, numerous studies have been undertaken to improve our knowledge of OCS vegetation uptake (e.g., [5-12]).

Despite its high tropospheric abundance and this increased interest, large uncertainty remains in both the OCS source and sink budgets. Watts [13] and Kettle et al. [3] proposed a mass budget described as balanced within the range of estimated uncertainty, but in fact it is imbalanced with sinks higher than sources. More recent modeling studies [5,8,14] suggested an additional oceanic source concentrated in the tropics to balance the increased global vegetation sink required to reproduce the seasonal variation observed in atmospheric concentration measurements.

Stratospheric sulfate aerosol (SSA) is important for a number of processes that affect the chemical and radiation balance of the atmosphere: heterogeneous chemistry reducing ozone, stratospheric warming and tropospheric cooling [15]. Crutzen [4] was the first to suggest that photodissociation of OCS may contribute significantly to the non-volcanic background sulfate layer in the stratosphere discovered by Junge et al. [16]. Because OCS is relatively inert in the troposphere it can be transported into the stratosphere where it is broken down by photodissociation through the absorption of ultraviolet sunlight. Other sulfur-containing gases such as sulfur dioxide (SO_2) contribute also to SSA, but the contribution of each one is uncertain. Some model and isotopic fractionation studies (e.g., [17-20]) suggested that production of SSA from OCS oxidation is too small to maintain the SSA background level and proposed that SO_2 transported from the troposphere is the most important precursor for the SSA layer, allowing for the possible influence on SSA by human emissions. However, several recent papers are in disagreement with this view [21-23]. The most recent one [24] estimated that OCS supplies about 56% of the background SSA burden, suggesting that upward transport of OCS from the troposphere largely controls the sulfur budget and the aerosol loading of the background stratosphere.

The lack of any substantial trend in OCS atmospheric loading over the last decades of the 20th century (e.g., [25]) was consistent with a balanced mass budget within the range of estimated uncertainty. This 'no-trend' argument was also used in the discussion about the contribution of OCS to SSA, when compared with the increasing trend observed in stratospheric aerosol loading since 2002 (e.g., [26]). However, a small (less than 1% per year) but statistically significant long-term decrease was reported from ground-based infrared measurements recorded above Jungfraujoch (Swiss Alps) from 1990 to 2002 ([27], also noticed by Rinsland et al. [25], above Kitt Peak in Arizona between 1978 and 2002). The updated Jungfraujoch data set revealed an increase of OCS over 2002–2008. More recently, Kremser et al. [28] have observed positive trends in their ground-based infrared measurements recorded at three Southern Hemisphere sites from 2001 to 2014. At a more global scale, a relatively small positive trend in global OCS derived from surface observations (1.8 pptv per year) was also reported in the WMO Scientific Assessment of Ozone Depletion (2010) for the period 2000–2008 [29] and recent observations from the NOAA (National Oceanic and Atmospheric Administration) surface network updated through 2012 suggest that any systematic changes in global OCS since 2000 have been small (less than 3%), with an increase of 0.4% from 2011–2012 [1].

The impact of OCS anthropogenic emissions on the abundance of atmospheric OCS is another matter of debate in the scientific community. Turco et al. [30] estimated that increasing anthropogenic emissions of OCS could cause measurable climate alterations within the next century. The anthropogenic part of global OCS sources has increased with time in the global mass budgets, from less than 25% in 1984 [31] to about 40% in 2002 [3], with oxidation of industrial CS_2 emissions as the main contributor. Using campaign-type atmospheric measurements above the western Pacific region, Blake et al. [32] observed that air masses of Chinese and Japanese origin were characterized by high OCS mixing ratios coming from land-based sources, suggesting underestimated Chinese emissions (most likely because emission ratio from Chinese coal burning is poorly characterized). A new global anthropogenic inventory for the years 1850–2013 based on new emission measurements and material-specific data results in a smaller growth in the OCS anthropogenic source than previously estimated [33]. Derived from ice and firn air analyses, the history of OCS atmospheric mixing ratios since 1850 seems to be closely related to historical anthropogenic sulfur emissions [34].

Moreover, the slow and long-term increase in atmospheric OCS deduced from ice and firn data analysis on a large temporal scale could indicate a decline in terrestrial productivity [35], increasing the scientific interest for OCS as a proxy of the first global history of GPP [33].

In view of these studies, precise and long-term sets of tropospheric and stratospheric OCS measurements are needed for trend evaluation and to obtain insights into source and sink strengths and their geographic locations [25]. In this paper, we report on the evolution of the vertical carbonyl sulfide loading integrated over the free troposphere and stratosphere above the high-altitude Jungfraujoch station, derived from the spectrometric analysis of Fourier transform infrared (FTIR) solar observations made at that site between 1995 and 2015. Related findings are compared with new in situ gas chromatography mass spectrometry (GCMS) measurements performed by Empa (Laboratory for Air Pollution/Environmental Technology) at the Jungfraujoch since 2008, as well as with space-borne solar occultation observations performed by the ACE-FTS instrument on-board the SCISAT satellite.

With respect to the previous ground-based FTIR work, the present analysis has been performed with a new optimized retrieval strategy, mainly an updated set of microwindows and line parameters, with the goal of providing a more accurate and extended time series of tropospheric and stratospheric abundances, long-term trends and seasonal variations.

Please cite this article as: Lejeune B, et al. Optimized approach to retrieve information on atmospheric carbonyl sulfide (OCS) above the Jungfraujoch station and change in its abundance since 1995. J Quant Spectrosc Radiat Transfer (2016), http://dx.doi.org/10.1016/j.jqsrt.2016.06.001

2. Instrumentation and data sets

2.1. FTIR remote-sensing measurements and retrieval strategy

The long-term OCS time series presented and analyzed in this study has been derived from the analysis of solar spectra recorded between January 1995 and July 2015 under clear-sky conditions at the high-altitude International Scientific Station of the Jungfraujoch (hereafter JFJ; Swiss Alps, 46.5°N, 8.0°E; 3580 m above sea level). The recordings were made with a high spectral resolution Fourier transform infrared spectrometer (Bruker-120 HR). Since 1990, the University of Liège research activities at JFJ are performed within the frame of the Network for the Detection of Atmospheric Composition Change (NDACC; see http://www.ndacc.org; e.g., [36]).

The initial database investigated here consists of about 6600 spectra recorded with an optical filter covering the 1800 to 2250 cm^{-1} spectral region including the strongest infrared band of OCS – ν_3 centered at 2062 cm^{-1}. Spectral resolutions (defined as the reciprocal of twice the maximum optical path difference) alternate between 0.0029 and 0.0044 cm^{-1} depending on the rate of solar zenith angle variation during the day, and the scanning time of successive recordings. Signal-to-noise (S/N) ratios vary between 100 and more than 6500 (average spectra resulting from successive individual Bruker scans, predominantly around midday, when solar zenith angles vary slowly).

The spectral analyses were performed with the SFIT-2 v3.91 fitting algorithm, a code based on the optimal estimation method (OEM) formalism of Rodgers [37] and specifically developed to retrieve vertical column abundances and mixing ratio profiles of atmospheric gases from FTIR observations [38]. This code has been successfully compared with the PROFFIT retrieval algorithm [39,40], the other tool in use by the NDACC FTIR community, showing consistent results for numerous tropospheric and stratospheric target gases.

Line parameters adopted in the spectral fitting process were taken from the HITRAN 2012 spectroscopic compilation [41], supplemented with an empirical OCS linelist produced by G.C. Toon from Jet Propulsion Laboratory, California Institute of Technology in Pasadena (personal communication, 2014) and containing 709 weak OCS lines belonging to two bands that are missing from HITRAN 2012. With respect to the retrieval strategy described in this paper, the use of the HITRAN 2008 [42] or HITRAN 2004 [43] compilation degrades the fitting residuals by 5.5 and 13.1%, respectively (for the 399 spectra recorded in 2009).

The model atmosphere adopted above the 3.58 km Jungfraujoch altitude consists of a 39 layer scheme with progressively increasing thickness to reach 100 km altitude. The pressure–temperature profiles are those specifically computed for the JFJ location and noontime on a daily basis by the National Centers for Environmental Prediction (NCEP, Washington, DC; see http://www.ncep.noaa.gov).

The stratospheric portion of the a priori Volume Mixing Ratio (VMR) OCS profile was deduced from a set of 101 solar occultations performed between March 2004 and October 2012 in the $\pm 5°$ latitude and $\pm 10°$ longitude zone around the JFJ location by the Atmospheric Chemistry Experiment Fourier Transform Spectrometer (ACE-FTS; [44,45]). We assumed a constant tropospheric mixing ratio with the 9.5 km ACE-FTS value (450 pptv) extended down to the JFJ altitude. Diagonal values of the covariance matrix and the Gaussian half width for interlayer correlation (2 km) adopted for off diagonal elements are also based on these ACE-FTS measurements. Note that the assumption of a constant tropospheric mixing ratio is consistent with previous measurements and OCS long tropospheric lifetime [25] and is supposed to correctly represent the mean of the different profiles linked to the plant uptake seasonal variations.

For all interfering molecules, averaged VMR profiles based on WACCM (the Whole Atmosphere Community Climate Model, e.g. [46]) model predictions for the 1980–2020 period and the JFJ station were used, except for H_2O (WACCM values divided by 5.0 to get closer to the a priori profile used by Sussmann et al. [47]) and for CO (composite profile using WACCM and ACE-FTS values, for details see [48]). All these a priori VMR profiles are simply scaled during the fitting procedure, except for O_3 (vertical profile retrieved with the covariance matrix described by Barret et al. [49]). Solar lines come from the empirical line-by-line model developed by Hase et al. [50]. We adopted a S/N ratio of 300 for inversion throughout the spectral fitting calculations, after testing different values in order to optimize the fitting residuals while avoiding unphysical oscillation in the retrieved profiles. This S/N ratio is used as a regularization parameter for the OEM, as described, e.g., in Section 2.2 of [51].

The first selection of a spectral region optimized for OCS column retrieval from ground-based FTIR measurements was described by Rinsland et al. [52] who used two microwindows centered on the P(37) and P(15) lines of the OCS ν_3 fundamental band, which is about 2 orders of magnitude stronger than any other OCS IR band. These lines were judged as the best ones, in particular because they are least affected by interference due to several other telluric gases, mainly H_2O, CO_2, O_3, and CO, and by lines of the $\Delta v=1$ vibration-rotation sequence of solar CO. In 2002, Rinsland et al. [25] proposed an updated strategy with three microwindows using P(37), P(25) and P(15) as target lines. Since then, to our knowledge no description of a new set of microwindows has been published. Krysztofiak et al. [53] opted for a 4-windows approach but without explanation of their specific choice. Considering the recent growing interest in scientific community in OCS and the progress made in computer performance and improved spectroscopic data for the target and interfering species, we have decided to revisit the OCS retrieval strategy and systematically explore the entire ν_3 fundamental band in order to determine an updated approach optimizing the information content while minimizing the associated error budget.

We started from a simulated solar spectrum to serve as an appropriate basis for the line selection, i.e.

Please cite this article as: Lejeune B, et al. Optimized approach to retrieve information on atmospheric carbonyl sulfide (OCS) above the Jungfraujoch station and change in its abundance since 1995. J Quant Spectrosc Radiat Transfer (2016), http://dx.doi.org/10.1016/j.jqsrt.2016.06.001

representative for the conditions prevailing at the dry high altitude site of the Jungfraujoch. Note that 2009 is selected as the reference year for simulation and for upcoming line tests. We chose the 1st of October for the pressure–temperature profile since that day shows representative values with respect to the annual means for air temperature and pressure at the Jungfraujoch altitude, as well as for the tropopause altitude. We used the same input parameters as for the retrievals used in this paper, except for the VMR profile of H_2O which is scaled to correspond to the 75th-percentile (P75) for water vapor total columns observed above Jungfraujoch in 2009 (129 observation days; see [47], for details about the H_2O retrieval strategy and time series). We selected P75 instead of the mean water vapor column so that the lines selection remains optimal even in wet conditions for that site.

The OCS ν_3 fundamental band includes 235 transitions from P(117) to R(117) for the main isotopologue $^{16}O^{12}C^{32}S$ in the 1998.47–2092.68 cm^{-1} spectral region [41]. To be considered in our study, a line must absorb at least 1% of the signal even for small air mass conditions. So we first simulated a spectrum with a solar zenith angle (SZA) corresponding to the 10th-percentile for the 2009 SZA values (38.6°). This allowed us to select a subset of 117 lines from P(58) to R(58). For further line selection, we simulated a spectrum with a SZA of 72.4° corresponding to the 50th-percentile for the 264 lower resolution (0.0044 cm^{-1}) spectra of 2009 (which are more represented in the database, with about 50 more observation days than for high resolution spectra). At this stage of the selection process, the wavenumber limits of all the microwindows (abbreviated mw's hereafter) used for the evaluation of the 117 lines are determined systematically by taking half of the difference between two successive OCS lines. Widths of the resulting mw's range from 0.54 to 0.26 cm^{-1}.

To establish an objective ranking of all the microwindows as a function of the estimated quality of the OCS line fitting, we have constructed a coefficient (simply named COEFF) taking into account the parameters affecting/perturbing the proper functioning of the SFIT-2 code, namely

(i) the interferences absorption level: for each simulated spectrum point of the considered mw, we added up the relative absorption of each interference at this point (normalized to its mw minimal absorption), according to the maximum OCS absorption in the mw.
(ii) the background signal: for each mw we added up the minimum absorption of each interference (the visibility of the target line in the spectrum is impacted by the absorption of even an horizontal background signal).

The COEFF for a considered mw is determined by the sum of the interference absorptions (divided by the number of points used) and the background signal. Interferences considered are O_3, CO_2, H_2O, CO and solar lines. In the specific case of saturated absorption (no transmission), we directly set the absorption term to the value 1 without normalization.

For each mw, we focused on the immediate vicinity of the OCS target line center by using a filter which only considered the middle part of the mw (first and last quarter of the mw are rejected) and points where OCS absorption is at least 10% of the maximum OCS absorption of the mw. This allows us to avoid taking into account weaker OCS lines simulated from other isotopologues and/or transitions and to ignore interferences in the external

Table 1
List of primary target lines, respective microwindows, principal telluric interferences and COEFF values.

Line	OCS line position	Microwindow	Interfering gases	COEFF	Comments
P(15)	2055.860551	2055.64–2055.96	O_3, CO_2	0.26	[25]
P(25)	2051.331396	2051.17–2051.49	O_3, CO_2, H_2O	0.30	[25]
P(32)	2048.017611	2047.85–2048.22	O_3, CO_2	0.34	
P(22)	2052.715469	2052.49–2052.91	O_3, H_2O	0.43	
P(28)	2049.925642	2049.77–2050.16	O_3, CO_2, H_2O, CO	0.44	
P(21)	2053.172006	2053.08–2053.36	O_3, CO_2, H_2O	0.47	
P(11)	2057.604594	2057.43–2057.79	O_3, CO_2, H_2O	0.48	
P(37)	2045.578490	2045.33–2045.69	O_3, CO_2	0.49	[25]
P(31)	2048.498227	2048.22–2048.74	O_3, CO_2, H_2O	0.56	
P(29)	2049.452242	2049.29–2049.61	O_3, CO_2	0.57	
P(19)	2054.077843	2053.99–2054.24	O_3, CO_2, H_2O, CO	0.58	
P(50)	2038.956156	2038.85–2039.19	O_3, CO_2	0.61	
R(24)	2071.550841	2071.34–2071.75	O_3, CO_2	0.67	
R(14)	2067.994318	2067.83–2068.18	O_3, H_2O	0.68	
P(18)	2054.527142	2054.33–2054.74	O_3, CO_2, H_2O	0.69	
P(34)	2047.049170	2047.00–2047.28	O_3, CO_2, H_2O	0.72	
R(25)	2071.892978	2071.75–2072.00	O_3, CO_2, H_2O	0.72	
P(8)	2058.887220	2058.68–2059.01	O_3, CO_2, H_2O	0.73	
P(12)	2057.172211	2057.01–2057.33	O_3, CO_2	0.73	
P(14)	2056.300189	2056.15–2056.43	O_3, CO_2	0.74	
R(15)	2068.361008	2068.18–2068.55	O_3, CO_2	0.74	

Microwindows are ranked by their COEFF value. We removed mw's with a COEFF exceeding the mean+1σ value and then only considered the 20th-percentile remaining best values for further evaluations. Position (from HITRAN 2012 compilation) and limits of the microwindows are in cm^{-1}. All target OCS lines are in the ν_3 vibration-rotation band. Please note that COEFF values have been determined before mw's edges adjustments.

Please cite this article as: Lejeune B, et al. Optimized approach to retrieve information on atmospheric carbonyl sulfide (OCS) above the Jungfraujoch station and change in its abundance since 1995. J Quant Spectrosc Radiat Transfer (2016), http://dx.doi.org/10.1016/j.jqsrt.2016.06.001

parts of the OCS line wings which disturb the fits less. Comparison to the maximum OCS absorption in the mw (instead of the absorption at the considered point) minimizes the relative absorptions of the filtered interferences not placed in the center region of the target line. The division of each mw absorption term by the number of points used cancels out the influence of the mw size. The monochromatic point spacing used for the simulation was 0.0013 cm^{-1}.

COEFF values are used to select mw's on which the fitting tests are to be performed. We removed mw's with a COEFF exceeding the mean$+1\sigma$ value and chose to work with the 20th-percentile best values, for a total of 21 mw's. Table 1 lists these selected mw's ranked by their COEFF value. The edges of the mw's have been adjusted to avoid strong modulation of the absorption near the mw's borders. The three mw's used by Rinsland et al. [25] are among the best ones, giving us confidence in the robustness of our selection method.

Fig. 1 shows for these 21 mw's the results of the fitting for the 399 spectra from 2009. The average root mean square (RMS) residuals (differences between observed and fitted spectra) are plotted as a function of the information content (Degree Of Freedom for Signal – DOFS; the trace of the averaging kernel matrix; see [54]). All mw's are included in the same DOFS interval (roughly between 1.5 and 2.5), except for the P(50) line. For the residuals, the dispersion is much greater with RMS values from 0.1 to 0.6. Since the goal of this study is to improve the current OCS retrieval strategy, we decided to focus on mw's with better residuals than the P(15) and P(37) lines used by Rinsland et al. [25] which are both affected by the presence of a strong solar line. P(50) and P(34) are rejected, given their low DOFS level and the fact that they don't allow extending higher up the altitude sensitivity range of the measurements (illustrated on Fig. 4). Therefore, next step of the selection deals with the mw's associated with the P(32), P(31), P(28), P(25), P(21), P(19) and P(18) target lines.

Subsequently, we fitted all possible pairs including the P(25) line (which is the best one from the point of view of residuals – see Fig. 1). Residuals obtained for each mw in combination are compared with those obtained individually and the mean resulting residuals degradations are computed. The P(25)–P(31) association is the only one to exceed 30% degradation (mean value for the six combinations: $18.1 \pm 8.4\%$) and P(31) is thus rejected.

Griffith et al. [55] used the same spectral regions as Rinsland et al. [52] for their study of the inter-hemispheric ratio in OCS columns to minimize systematic differences between both analyses, but they found systematic differences in the OCS columns between the two mw's centered on the P(15) and P(37) lines for the spectra recorded in Lauder and Wollongong. In contrast to the high-altitude sites of Kitt Peak and Jungfraujoch where air masses are drier, the sites of Lauder (370 m) and Wollongong (35 m) are more perturbed by H_2O absorption features. Griffith et al. deduced that the retrieved OCS columns are influenced by how the fitting procedure models the background level and curvature, and the H_2O wings in particular (as found for the P(37) line and not for the P(15) line). For that reason, we decided to test the behavior of each mw with regard to water vapor.

P(32) is not affected by H_2O; P(28), P(21) and P(19) contain H_2O wings; P(25) and P(18) include a H_2O line almost completely and are supposed to provide the best H_2O information. To decide which one will be used as a reference, we compared the retrieved H_2O total columns of P(25) and P(18) mw's with the one provided by a fit using a retrieval strategy specifically developed to obtain H_2O [47]. We only considered coincident measurements with a coincidence interval of 1 hour (276 data), given the high variability of H_2O with time. Results show a better correlation for P(18) with an R coefficient of 0.99 and a slope for the correlation line of 1.01 ± 0.01 (instead of 0.98 and 0.95 ± 0.01 for P(25)).

Fig. 2 illustrates the quality of the H_2O information provided by the different mw's when using the P(18) mw as reference. It is clear that H_2O information coming from the extremity of a wing leads to a poor correlation when compared with the P(18) reference information. On the other hand, the 2049.77 cm^{-1} starting point of the P(28) mw (upper-right frame of Fig. 2) allows substantial part of the wing to be included (about at half maximum of the line absorption for the solar zenith angle simulated here) and, as a result, improves the quality of the correlation. To optimize the representation of the background level and curvature by the fitting procedure, we decided to reject the P(21) and P(19) mw's and to adopt a four-microwindows strategy with P(32), P(28), P(25) and P(18) as target lines. They are illustrated in Fig. 3.

On this figure, we can see that characteristic absorptions of CO_2 in the P(32), P(25) and P(18) mw's are likely to also perturb the modeling of the background level and curvature (weak absorption lines in the mw's associated with a slope and/or curvature linked to nearby stronger lines). To limit the impact of these CO_2 interferences, we added a fifth mw dedicated to improving the CO_2 adjustment (notice that the main isotopologue $^{16}O^{12}C^{16}O$ and the $^{16}O^{12}C^{18}O$ isotopologue, present in the P(28) mw, have to be retrieved independently). This so-called 'CO_2 mw' provides enough information about $^{16}O^{12}C^{18}O$ to reach a correlation of 0.88 (slope of the correlation line: 1.02 ± 0.05) when we compare the deduced CO_2 total column (daily means of year 2009) with those coming from a specific CO_2 retrieval strategy developed by [56]. Without the dedicated 'CO_2 mw', the correlation gets worse ($R=0.43$, slope of 2.19 ± 0.42). When completely neglecting the fit of CO_2, the shape of the OCS vertical profile retrieved in the troposphere is altered, hence this option is unsatisfactory. A more robust CO_2 total column retrieval contributes to the quality of the OCS product, which is particularly important given their correlation in the troposphere (vegetation uptake).

Note that we have also made a distinction between $H_2{}^{16}O$ and $H_2{}^{18}O$ which are both present in the P(18) mw.

Table 2 summarizes the retrieval parameters finally adopted in this paper. The five selected microwindows are fitted simultaneously. For the 2009 spectra, results show an average DOFS of 2.75 ± 0.33. This corresponds to a significant improvement when compared to the approach used in [25] which, for the same spectra and line

Please cite this article as: Lejeune B, et al. Optimized approach to retrieve information on atmospheric carbonyl sulfide (OCS) above the Jungfraujoch station and change in its abundance since 1995. J Quant Spectrosc Radiat Transfer (2016), http://dx.doi.org/10.1016/j.jqsrt.2016.06.001

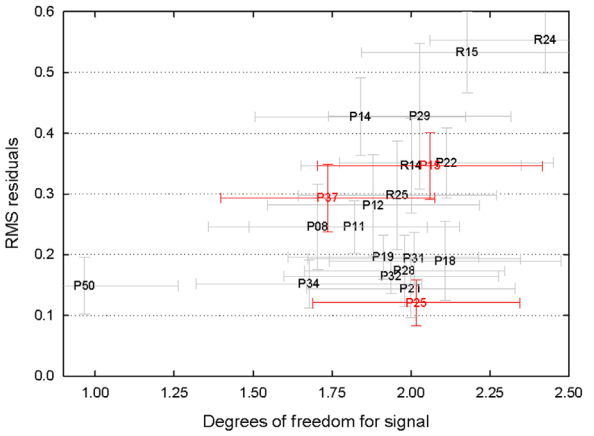

Fig. 1. Annual mean of Degrees of freedom for signal (DOFS) vs Root Mean Square (RMS) for residuals determined for the 21 mw's defined in Table 1 with the 399 JFJ spectra in 2009. Error bars correspond to the standard deviation around the mean values. Mw's used in [25] are shown in red.

parameters (HITRAN 2012), would provide an average DOFS of 1.98 ± 0.34.

Table 3 provides an error budget resulting from major instrumental and analytical uncertainties that may affect typical individual OCS total column amounts above the site. As described in [57], while most of the error terms have been dealt with using perturbation methods applied to all solar spectra recorded during the year 2009, the contribution of measurements noise, smoothing and forward model parameters to the random component have been computed following the OEM formalism of Rodgers [58] on the basis of a representative subset of solar spectra. The alternative a priori profile comes from version 3 of ATMOS [59] and is the zonal mean (40–49°N) observed during the 1994 mission (see Figure 2.9 in Chapter 2 of [15]).

The largest contribution to the total systematic error results from the spectroscopic uncertainties in line-intensities for OCS, estimated at 5% (for the target lines) in the HITRAN 2012 database that we have adopted for all retrievals in this study. In the HITRAN 2004 edition, the intensities of the ν_3 band of the principal isotopologue $^{16}O^{12}C^{32}S$ were increased by 15.79% [42] to match the average of the measurements reported by Regalia-Jarlot et al. [60] and Vander Auwera and Fayt [61] who set the 5% uncertainties mentioned above. Since then, there have been only minor revisions in the following editions.

2.2. GCMS in situ measurements

In situ atmospheric OCS measurements at JFJ have also been conducted using ground-based sampling and gas chromatography – mass spectrometry (GCMS) measurement techniques. These measurements are performed by Empa since 2008 using a Medusa-GCMS [62,63]. Two liters of sample are collected on a first cold trap (~ -160 °C) and cryo-focussed on a second trap before desorption into the GCMS. Air sample analyses are bracketed by standard gas (whole air samples) measurements to track and correct for detector sensitivity, leading to 2-hourly air measurements. Measurement precisions, as determined from the repeated standard analysis, are ~0.3%. The results are reported on a calibration scale used within the Advanced Global Atmospheric Gases Experiment (AGAGE), which was adopted from NOAA (see [34]).

3. Results and discussion

The strategy described in Section 2 has been applied to all available FTIR observations recorded with the Bruker instrument between January 1995 and July 2015. After exclusions of some observations (S/N ratios lower than 400, solar zenith angle higher than 85°, negative retrieved water vapor total column, bad residuals for solar lines, and outliers falling outside of the $+2.5\sigma$ confidence interval deduced from a non-linear regression fit of the residuals as function of the solar zenith angle), the database upon which the results and discussion are based includes 6334 individual OCS column measurements above JFJ, encompassing 2081 observational days.

Averaging kernels provide a direct assessment of the theoretical altitude sensitivity of the observations in the absence of errors in the measurements and model parameters [54]. They are a function of the retrieval intervals selected, the spectral resolution of the observations, an assumed S/N ratio for the inversion, and the selections of the retrieval parameters, such as the a priori profile and its covariance matrix. Fig. 4 shows that the altitude sensitivity of the FTIR measurements extends from the JFJ altitude (3.6 km) to about 25 km.

The mean DOFS of the dataset (2.79 ± 0.35) allows us to consider, in addition to the total column, a minimum of two partial columns. In fact, almost three partial columns are available, given the eigenvalues associated to the typical observation characterized in Fig. 4 (0.99, 0.96 and 0.70 for λ_1, λ_2, and λ_3, respectively). The λ_3 value means that 70% of the information is coming from the measurement for the corresponding eigenvector. Here however, we will focus on the two components and corresponding altitude ranges depicted in frame C of Fig. 4, in order to minimize as much as possible the impact of the region surrounding the tropopause (e.g., [25]), which is a mixture of tropospheric and stratospheric air. Note that the mean altitude of the tropopause above JFJ for the considered dataset is 11.7 km, with a 2σ of 2.5 km (calculated from the NCEP pressure–temperature profiles). Therefore we used two partial columns, making sure that the information is coming entirely from the measurements (96% for the second eigenvector) and enabling us to isolate tropospheric and stratospheric components of OCS. The selected merged layers (see Fig. 4, frame C) are 3.6–8.9 km and 13.8–19.5 km, with a tropopause which is out of these two altitude ranges for more than 92% of the total observational days.

Fig. 5 (bottom frame) reproduces the daily mean tropospheric vertical partial (3.6–8.9 km) column abundances (expressed in numbers of OCS molecules per square cm) derived above JFJ between 1995 and 2015.5.

Please cite this article as: Lejeune B, et al. Optimized approach to retrieve information on atmospheric carbonyl sulfide (OCS) above the Jungfraujoch station and change in its abundance since 1995. J Quant Spectrosc Radiat Transfer (2016), http://dx.doi.org/10.1016/j.jqsrt.2016.06.001

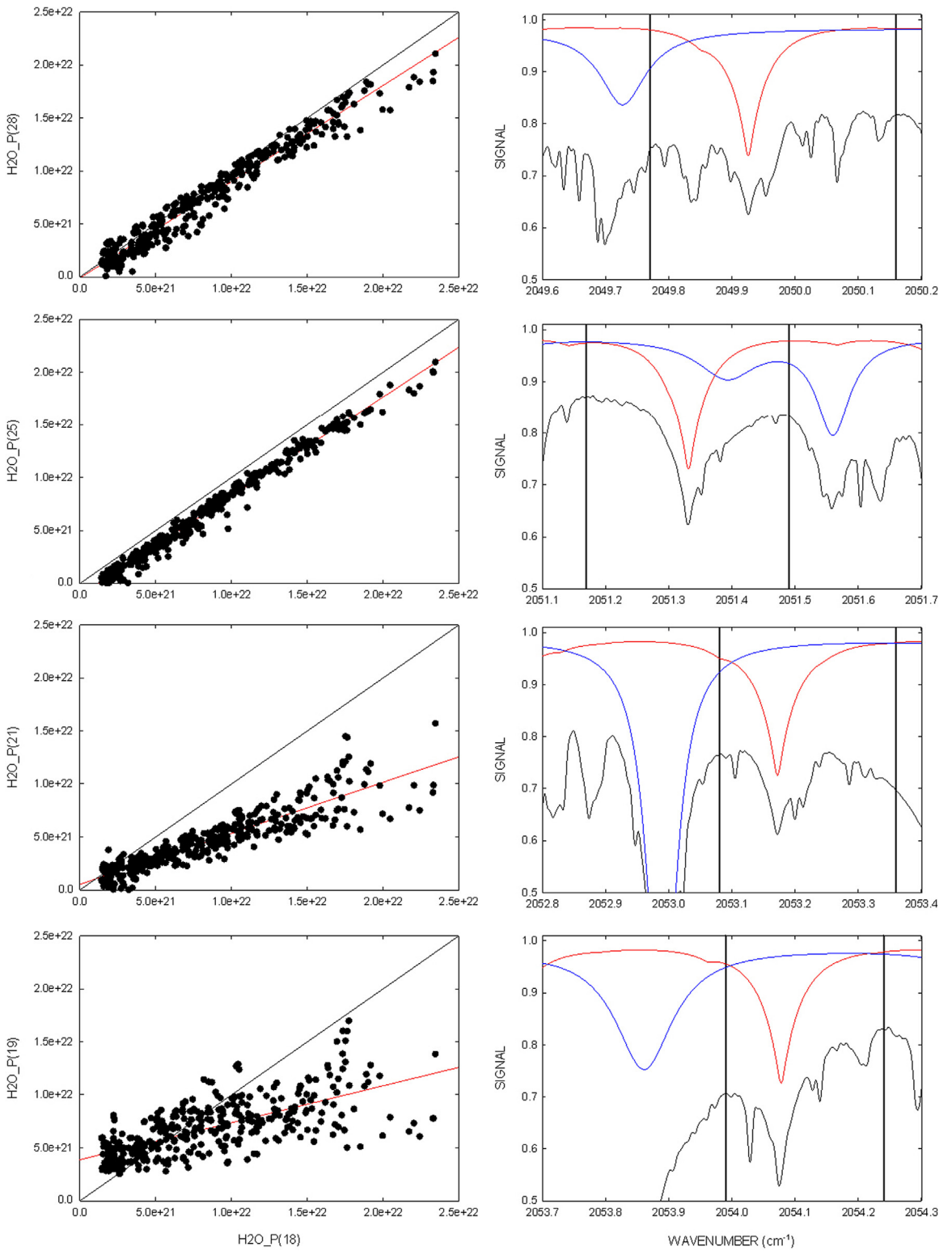

Fig. 2. Correlation between retrieved H_2O column deduced with P(28), P(25), P(21) and P(19) mw's when compared to those derived from the P(18) mw (left frames). Column values are expressed in molecules/cm². Black line is the ideal correlation (slope = 1) and red line is the correlation line. Right frames illustrate the H_2O absorption (blue curve) in a simulated spectrum (black curve) for P(28), P(25), P(21) and P(19) mw's (red curve is the OCS absorption). The simulation is representative of a typical spectrum recorded above JFJ (50th-percentile for the solar zenith angle and 75th-percentile for the H_2O column; percentiles are determined on the basis of the year 2009). Vertical black lines indicate the boundaries of the considered mw. (For interpretation of the references to color in this figure legend, the reader is referred to the web version of this article.)

Please cite this article as: Lejeune B, et al. Optimized approach to retrieve information on atmospheric carbonyl sulfide (OCS) above the Jungfraujoch station and change in its abundance since 1995. J Quant Spectrosc Radiat Transfer (2016), http://dx.doi.org/10.1016/j.jqsrt.2016.06.001

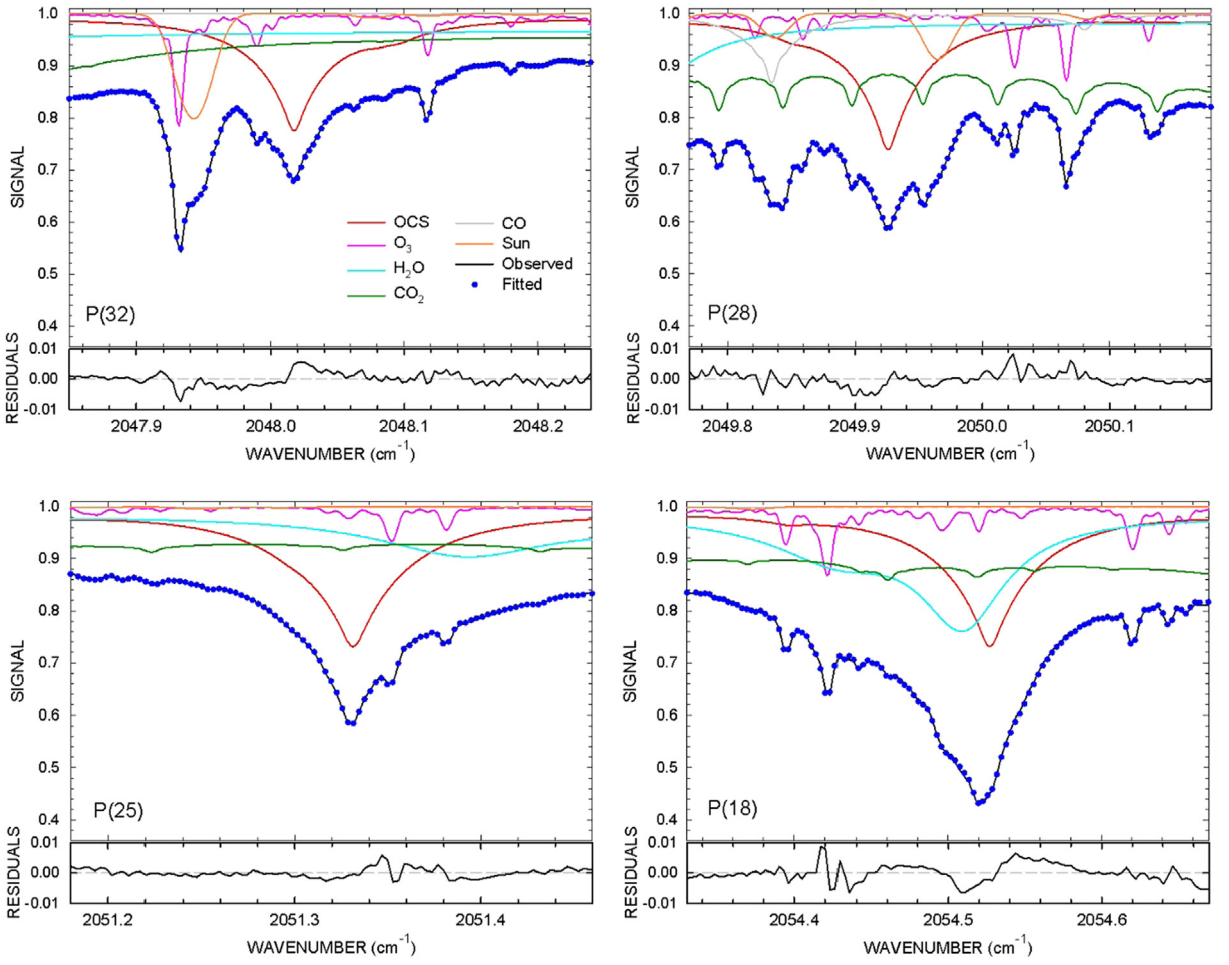

Fig. 3. Characteristic absorptions of OCS and the five most significant interfering gases (four telluric and one solar; see color key for their identification) in the four OCS microwindows selected for our retrievals, computed for a typical observation on 1 October 2009 (at 72.4° apparent solar zenith angle). Black trace represents the corresponding observed spectrum and the blue dots show the fitted spectrum. Residuals illustrated at the bottom of each frame correspond to the difference between observed and fitted signals. They all show differences of about 1%. (For interpretation of the references to color in this figure legend, the reader is referred to the web version of this article.)

Table 2
Summary of some of the retrieval parameters adopted in the present study.

Microwindow	OCS target line	Gases fitted
2030.75–2031.06	–	$^{16}O^{12}C^{16}O$ (s), O_3 (f)
2047.85–2048.24	P(32)	OCS (f), O_3 (f)
2049.77–2050.18	P(28)	OCS (f), O_3 (f), CO (s), $^{16}O^{12}C^{18}O$ (s)
2051.18–2051.46	P(25)	OCS (f), O_3 (f), $H_2{}^{16}O$ (s)
2054.33–2054.67	P(18)	OCS (f), O_3 (f), $H_2{}^{16}O$ (s), $H_2{}^{18}O$ (s)

(f): vertical profile fitted; (s): vertical profile simply scaled.

At first glance, three distinct periods emerge from Fig. 5, namely

(i) a first decreasing period of the OCS tropospheric loading above JFJ between 1995 and 2002, corresponding to a significant trend of (-0.89 ± 0.08) % yr^{-1} when referenced to 1995.

(ii) an intermediate increasing period from 2002 to 2008, during which the OCS tropospheric abundance returns to the level of 1995, with a significant trend of $(+1.34 \pm 0.08)$ % yr^{-1} (referenced to 2002).

(iii) and the more recent period which shows no significant trend since 2008.

These trends were determined by application of the statistical bootstrap re-sampling tool developed by Gardiner et al. [64]. This tool allows calculation, at the 2σ confidence level, of a long-term linear component, accounting for the seasonal modulation of a given data set with a third-order Fourier series.

Although also visible in the OCS total column abundances (see Table 4), these trends are clearly linked to/driven by tropospheric processes, given the lack of similar trends in the stratospheric partial column abundances.

The conversion of our measured OCS tropospheric column abundances into mean mixing ratios (as returned by the SFIT-2 code on the basis of the physical *P*–*T* model

Please cite this article as: Lejeune B, et al. Optimized approach to retrieve information on atmospheric carbonyl sulfide (OCS) above the Jungfraujoch station and change in its abundance since 1995. J Quant Spectrosc Radiat Transfer (2016), http://dx.doi.org/10.1016/j.jqsrt.2016.06.001

atmosphere adopted for each day) averaged for the tropospheric altitude range (from 3.6 to 8.9 km), allows some comparison with ground-level in situ measurements (GCMS) performed at JFJ by Empa. Note that the FTIR mixing ratios correspond to moist air values while the GCMS results are reported as dry air mole fractions. However this difference is insignificantly small for the present comparison because of the generally very dry air masses at JFJ, in particular at high altitude [65].

Table 3
Major sources of random and systematic errors on typical individual OCS total column retrievals above the Jungfraujoch.

Error sources	Error (%)	Comments
Systematic errors		
Line intensity OCS	5.6	Assuming the maximal HITRAN 2012 uncertainties
Air-broadening coefficient OCS	2.0	Assuming the maximal HITRAN 2012 uncertainties
Line intensity interfering gases	1.9	Assuming the maximal HITRAN 2012 uncertainties for O_3, H_2O, CO_2 and CO, combined in quadrature
Instrumental line shape	0.2	$\pm$ 10% misalignment and instrument bias
Forward model	1.0	Retrieval algorithm-related
OCS a priori profile	0.3	Assuming OCS a priori profiles derived from ACE-FTS and ATMOS
TOTAL SYSTEMATIC	6.3	
Random errors		
Temperature profile	0.5	Assuming the NCEP profile uncertainty pattern
H_2O a priori profiles	0.2	Changes by a factor of 2 in a priori slope
Solar zenith angle	0.5	Assuming $\pm 0.1°$ bias
Measurement noise	0.7	[58]
Smoothing	0.5	[58]
Model parameters	1	[58]
TOTAL RANDOM	1.5	

Fig. 6 illustrates (upper frame) the daily means OCS mixing ratios time series from FTIR and GCMS measurements, which are derived from ~600 coincident measurement days. The major difference between the two measurements is that the FTIR is a column measurements and hence representative of a large part of the free troposphere while the GCMS measurements are made on ground-based samples at this site and hence are more sensitive to local and short-term injection of polluted air masses. The average relative difference between FTIR and GCMS observations is (-4.8 ± 3.5) %, and this value is well within the systematic uncertainty estimated for the FTIR data (6.3%; see Table 3). The lower FTIR values are consistent with the general shape of the OCS vertical profile in the northern hemispheric mid-latitudes (see Fig. 4 in [66]) showing a decrease of the VMR's with elevation. A shift in the timing of the seasonal variation is also visible, or in other words, there is seasonality in the differences (see the upper part of the upper frame of Fig. 6). The maximum is reached almost at the same time for FTIR and GCMS observations (around mid-April and beginning of May), but a delay of 2 months is found for the minimum (in mid-September for GCMS and in mid-November for FTIR). GCMS and FTIR data are close to each other in summer, because of a faster decline in GCMS OCS (probably due to a shorter response time to detect the effect of the OCS vegetative uptake during the growing season). The peak-to-peak amplitude deduced from the seasonal cycle is

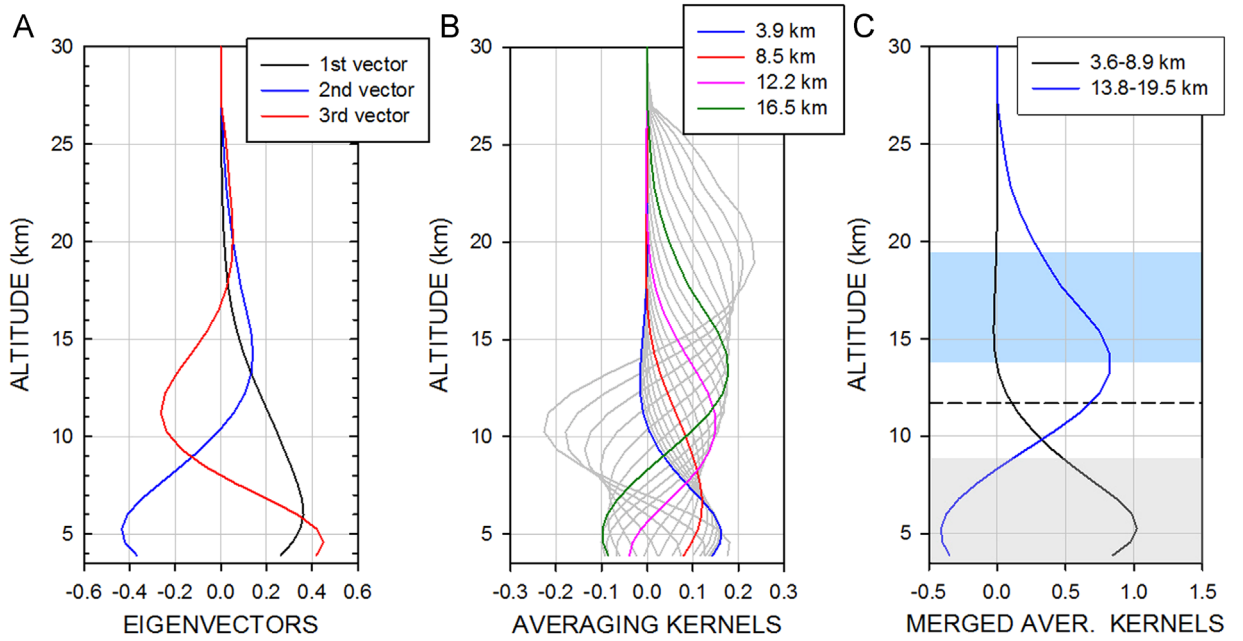

Fig. 4. First eigenvectors (A), layer averaging kernels (B) and merged averaging kernels (C) characterizing the FTIR retrievals of OCS above Jungfraujoch. These information parameters are deduced from a typical observation. Averaging kernels are normalized for the partial columns. Dashed line in frame C represents the mean tropopause altitude above JFJ and the blue and grey shaded bands illustrate the altitude range of selected tropospheric and stratospheric partial columns. (For interpretation of the references to color in this figure legend, the reader is referred to the web version of this article.)

Please cite this article as: Lejeune B, et al. Optimized approach to retrieve information on atmospheric carbonyl sulfide (OCS) above the Jungfraujoch station and change in its abundance since 1995. J Quant Spectrosc Radiat Transfer (2016), http://dx.doi.org/10.1016/j.jqsrt.2016.06.001

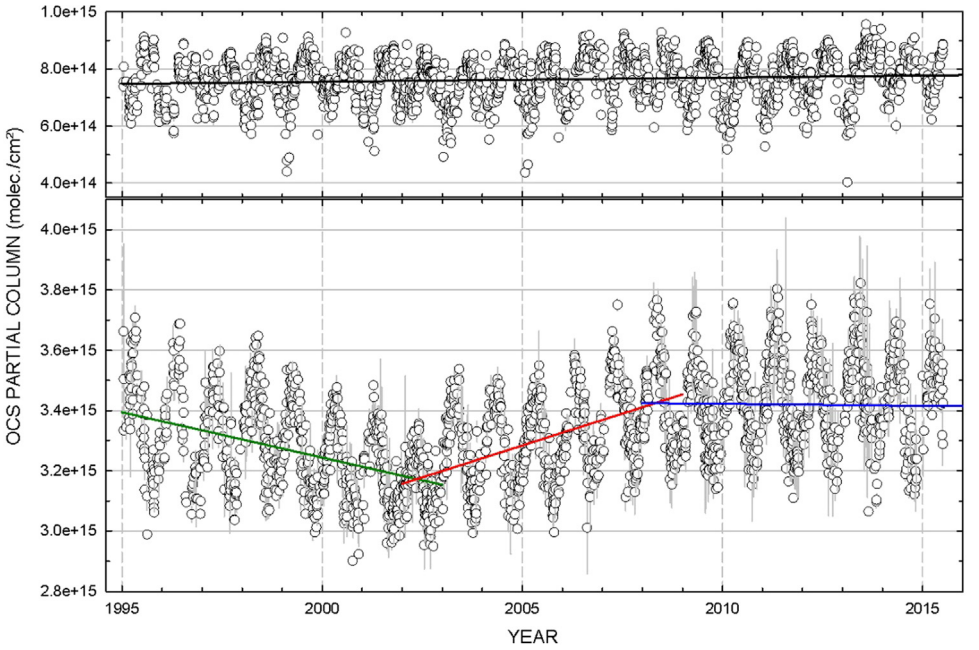

Fig. 5. FTIR time series of OCS daily mean vertical partial column abundances above the Jungfraujoch (expressed in numbers of OCS molecules per square cm). Upper frame concerns the stratospheric partial column (13.8–19.5 km) and bottom frame the tropospheric partial column (3.6–8.9 km). Error bars correspond to standard deviations around daily means. Green, red and blue lines in the bottom frame represent the trend line calculated by the statistical bootstrap resampling method from [64] for the 1995–2002, 2002–2008 and 2008–2015.5 time periods, respectively. The black one in the upper frame is for the 1995–2015.5 period. (For interpretation of the references to color in this figure legend, the reader is referred to the web version of this article.)

Table 4
Trends for OCS total, tropospheric and stratospheric columns above JFJ for different and relevant time periods deduced from our FTIR observations.

Trend unit	1995–2015	1995–2002	2002–2008	2008–2015
Total column				
molec. cm^{-2} yr^{-1} $\times 10^{13}$	$+1.75 \pm 0.14$	-3.67 ± 0.47	$+6.84 \pm 0.54$	$+1.40 \pm 0.56$
% yr^{-1}	$+0.31 \pm 0.03$	-0.62 ± 0.08	$+1.21 \pm 0.10$	$+0.23 \pm 0.10$
Tropospheric column (3.6–8.9 km)				
molec. cm^{-2} yr^{-1} $\times 10^{13}$	$+1.04 \pm 0.08$	-3.01 ± 0.25	$+4.24 \pm 0.25$	-0.14 ± 0.29
% yr^{-1}	$+0.32 \pm 0.03$	-0.89 ± 0.08	$+1.34 \pm 0.08$	-0.04 ± 0.08
Stratospheric column (13.8–19.5 km)				
molec. cm^{-2} yr^{-1} $\times 10^{13}$	$+0.15 \pm 0.04$	–	–	–
% yr^{-1}	$+0.20 \pm 0.06$	–	–	–

All trends are calculated with the statistical bootstrap re-sampling method developed by [64]. The reference value for the relative trends (% yr^{-1}) is the one calculated for the first point of the considered time period.

about 10%, relative to the mean of the considered data set (11.1% for the GCMS results and 10.4% for the FTIR results).

We also plotted on Fig. 6 (red line, upper frame) the fitted function deduced with the daily mean OCS mixing ratios obtained when using the Rinsland et al. [25] inversion strategy. The agreement with GCMS data is clearly better with our approach which allows a better capture of the seasonal cycle.

We also compared the FTIR stratospheric partial columns recorded above JFJ with FTIR solar occultation measurements from a space-based platform. The red curve on Fig. 6 (lower frame) represents the fit of the stratospheric daily mean OCS partial columns between 14 and 20 km altitude, derived from over 1380 solar occultation measurements (Version 3.5 products; [67]) recorded in the 41.5° to 51.5° northern latitude zone between 2004 and 2012 with the ACE-FTS instrument on-board SCISAT. Note that ACE-FTS retrievals for OCS were performed with the HITRAN 2004 spectroscopic database and with a set of 12 mw's covering the P-branch of the ν_3 fundamental band, including the four target lines of our ground-based retrieval strategy. To avoid comparing different air masses, we only considered the coincident days of measurements included in the −2.0°W to 18.0°E longitudinal zone to determinate the relative differences illustrated on the upper part of the lower frame of Fig. 6. More data are needed to correctly discuss about the average relative difference between FTIR and ACE-FTS observations ($+7.6 \pm 5.5$) %, deduced with less than 30 values. There is a nice agreement between the two data sets for the phase of the noticed seasonal cycle, although a small shift for the seasonal minimum is visible. Barkley et al. [66] suggested that atmospheric transport could be the seasonal process which influence the

Please cite this article as: Lejeune B, et al. Optimized approach to retrieve information on atmospheric carbonyl sulfide (OCS) above the Jungfraujoch station and change in its abundance since 1995. J Quant Spectrosc Radiat Transfer (2016), http://dx.doi.org/10.1016/j.jqsrt.2016.06.001

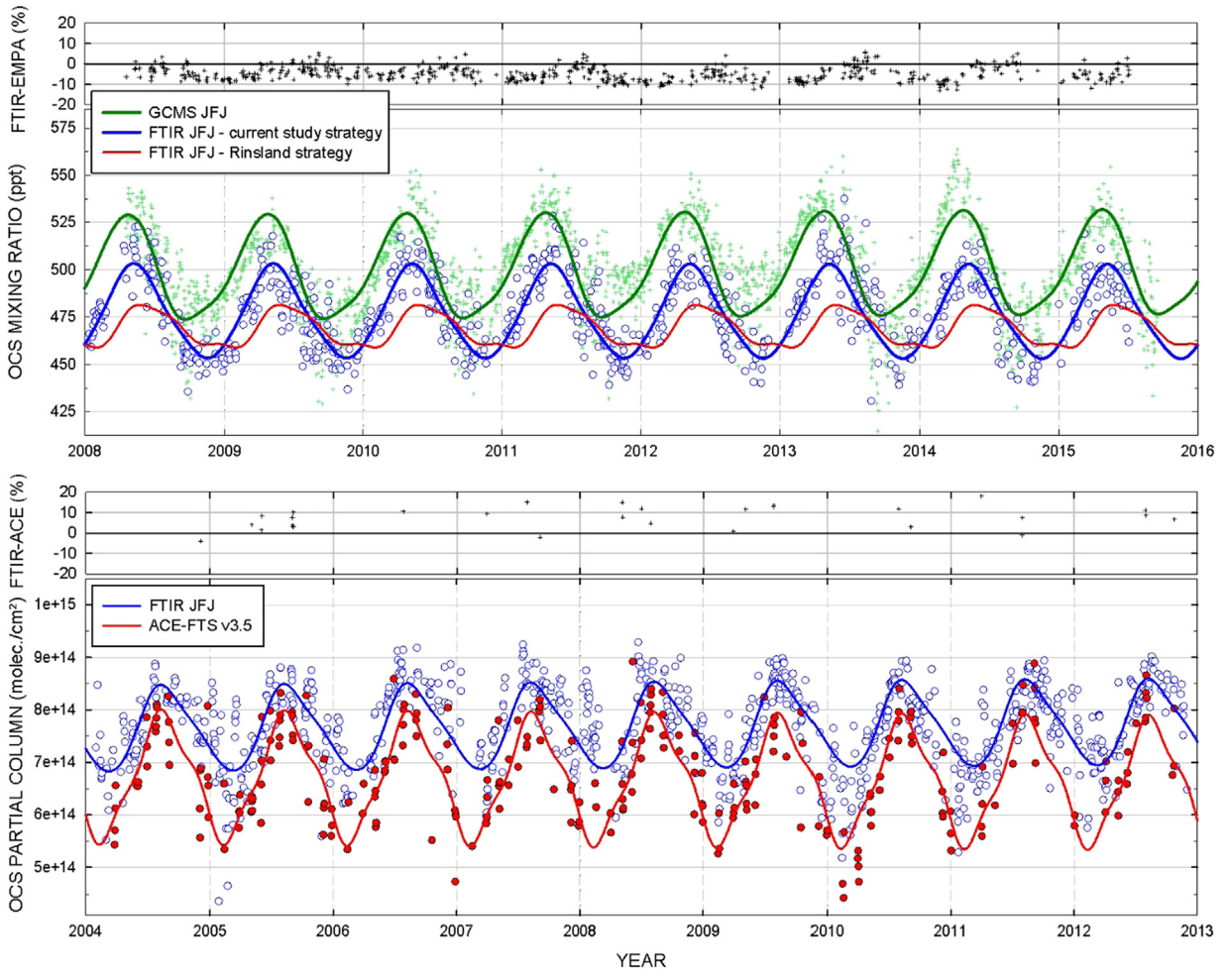

Fig. 6. Comparison of daily mean FTIR time series with in situ measurements (upper frame) and satellite observations (bottom frame). The time period under investigation result from data availability. Please note the different units used for the *y*-axis between the 2 frames. FTIR data in the upper frame correspond to the average mixing ratio of the 3.6–8.9 km altitude range, and in the bottom frame to the partial column covering the 13.8–19.5 km altitude range. The partial column of ACE-FTS corresponds to the 14–20 km altitude range. Blue, green and red dots follow the same key color that the curves which represent the fitted function coming from the statistical bootstrap resampling method from [64]. Relative differences for coincident days are illustrated with black crosses in the upper part of each frame. Red curve in the upper frame corresponds to the function fitted to the daily means OCS mixing ratios obtained with the [25] inversion strategy. (For interpretation of the references to color in this figure legend, the reader is referred to the web version of this article.)

stratospheric OCS concentrations. The contrasted amplitudes (21.4% for FTIR and about twice as large for ACE-FTS) are not presently understood but probably partially linked to the large spatial distribution of the satellite data. Mean latitudinal OCS profiles measured by ACE-FTS from 2004 to 2006 on a larger latitudinal zone (20°N–60°N; see [66]) show an amplitude of about 30% for the stratospheric (17 km) seasonal variation.

We compared the trends observed above JFJ with other OCS times series already published. The tropospheric decreasing trend of the 1995–2002 period (-0.89 ± 0.08) % yr^{-1} is slightly stronger than the one deduced by Rinsland et al. [25] above Kitt Peak (-0.25 ± 0.04) % yr^{-1} but the latter characterized a longer period (1978–2002), with a possible smoothing effect on the trend value. The decline of OCS concentration at the end of the 20th century has been noticed in both hemispheres from firn air and ice core analysis [34,68]. Our trend agrees with the (-0.8 ± 0.5) % yr^{-1} deduced by Sturges et al. [68] from firn air sampled at Devon Island (Canada) and for the 1988-1998 time frame. Diminution of CS_2 emissions by the viscose-rayon industry was mentioned as a possible cause for this trend.

For the tropospheric increasing trend of the 2002–2008 period, we can compare it with those reported by Kremser et al. [28] above Lauder and Wollongong from FTIR ground-based measurements in the Southern Hemisphere. The authors also noticed a change in the trend around 2008. For Wollongong, a tropospheric trend of ($+0.99 \pm 0.04$) % yr^{-1} for the 2001–2008 period was reported, not very far from the ($+1.34 \pm 0.08$) % yr^{-1} determined above JFJ for the 2002–2008 period. A short decreasing period followed but there is an increasing trend of almost the same value from 2010, in contrast with our stable period above JFJ since 2008. The approximatively same temporal scenario also applies for Lauder, with less intense increasing trends of about 0.50% yr^{-1}.

Please cite this article as: Lejeune B, et al. Optimized approach to retrieve information on atmospheric carbonyl sulfide (OCS) above the Jungfraujoch station and change in its abundance since 1995. J Quant Spectrosc Radiat Transfer (2016), http://dx.doi.org/10.1016/j.jqsrt.2016.06.001

The trend calculated for all GCMS data is $(+0.08 \pm 0.06)$ % yr^{-1} for the 2008–2015 period, a consistent result considering the recent observations from the NOAA surface network updated through 2012, which suggest small changes in global OCS since 2000 (less than 3%), with an increase of 0.4% from 2011–2012 [1]. This result is in agreement with the stable period deduced from the FTIR dataset starting in 2008.

The new global OCS anthropogenic inventory developed by Campbell et al. [33, see Fig. 1] for years 1850 to 2013 shows that the decreasing period at the end of the 20th century was mainly driven by the decline of industrial CS_2 emissions (dominated by rayon production). Emissions from coal combustion began to also decline since about 1990 due to concern over the impacts of sulfur emission. The geographical shift in the production of rayon materials (with China being now the dominant producer, pushing the global rayon production to grow by 140% between 2002 and 2013), combined with the continuous increase of biomass burning and emission linked to aluminum production, are consistent with the change in trend observed above JFJ in 2002. Especially as emissions coming from coal combustion seems to rise again at this time. Also OCS coal emissions are scaled in time using SO_2 coal emissions, the last report of SO_2 emissions ([69, see Fig. 2]) tend to confirm us that the OCS signal recorded above JFJ is closely related to anthropogenic sulfur emissions as already noticed by Montzka et al. [34] from ice and firn air analyses.

Concerning the stratospheric trend, the slight increase of $(+0.20 \pm 0.06)$ % yr^{-1} for the 1995–2015 period above JFJ has two-thirds of its confidence interval included in the insignificant trend deduced from ACE-FTS data (-0.19 ± 0.42) % yr^{-1} (2004–2013). This is in good agreement with the lack of a significant temporal trend for the stratospheric OCS abundance for the 1978–2005 period deduced from a database of spectra collected with an airborne infrared spectrometer [70]. Rinsland et al. [71] came to the same conclusion from solar occultation measurements near 30°N latitude recorded by the ATMOS (1985 and 1994) and the ACE FTS (2004–2007) satellite instruments. Note that the JFJ stratospheric trend is quite similar to those recorded above Lauder and Wollongong by Kremser et al. [28] for the 2001–2015 period. It might be tempting to also compare the JFJ OCS stratospheric trend with the one for the SSA. Since about 2000, an increase of 4–7% per year in the aerosol backscatter in the altitude range of 20–30 km has been detected at Mauna Loa and Boulder [26] but it is certainly too early to draw any conclusion because the contribution of each sulfur gas entering the stratosphere is still a matter of debate in the scientific community.

4. Summary and conclusions

Carbonyl sulfide (OCS) is the most abundant sulfur-containing compound in the free troposphere. The main source of OCS is biogenic activity in the ocean, and uptake by leaves and soil are its main sinks. OCS has attracted attention for its contribution to the non-volcanic background stratospheric sulfate aerosol (SSA) layer and more recently for its potential to become a photosynthesis tracer. However, large uncertainties remain in the field of OCS research, e.g., its global mass budget, its relative contribution to SSA or the impact of anthropogenic emissions on its long-term trend.

Long-term time series of tropospheric and stratospheric OCS measurements are needed to improve our knowledge about source and sink strengths and their geographic locations. The aim of this paper is to establish a new optimized retrieval strategy to derive the evolution of the OCS loading from the analysis of ground-based solar absorption spectra. The entire ν_3 fundamental band of the main isotopologue $^{16}O^{12}C^{32}S$ spectral region (1998.47–2092.68 cm^{-1}) was systematically explored in order to determine an updated approach optimizing the information content while minimizing the perturbations by several interfering atmospheric gases (mainly H_2O, CO_2, O_3, and CO), and by solar CO. We opted for a four-microwindows approach with P(32), P(28), P(25) and P(18) as target lines, combined with a fifth one dedicated to improving the CO_2 adjustment.

This new strategy has been applied to a database of about 6350 solar absorption spectra (more than 2000 observational days) recorded between January 1995 and July 2015 at the high-altitude International Scientific Station of the Jungfraujoch (Swiss Alps, 46.5°N, 8.0°E; 3580 m above sea level) with a high spectral resolution Fourier transform infrared spectrometer. The increased information content from our optimized strategy allows us to consider a tropospheric and a stratospheric component restricted to the 3.6–8.9 and 13.8–19.5 km altitude ranges, minimizing the impact of seasonal changes in the tropopause height.

Three distinct periods emerge from tropospheric partial column, namely (i) a first decreasing period between 1995 and 2002, corresponding to a significant trend of (-0.89 ± 0.08) % yr^{-1} (2σ), (ii) an intermediate increasing period from 2002 to 2008, during which the OCS tropospheric abundance returns to the level of 1995, with a significant trend of $(+1.34 \pm 0.08)$ % yr^{-1} (2σ), and (iii) the more recent period which shows no significant trend since 2008. These results are consistent with previous studies that also found a decline of OCS concentration at the end of the 20th century in both hemispheres. In contrast, the intermediate increasing period noticed above JFJ is only reported in the Southern Hemisphere from ground-based FTIR measurements.

When accounting for the total systematic error of $\pm 6.3\%$ affecting the FTIR measurements, which is dominated by the uncertainty on the OCS spectroscopic parameters adopted here, our tropospheric mixing ratios are in good agreement with results derived from in situ GCMS measurements performed since 2008 by Empa at the Jungfraujoch site. A quite similar seasonal cycle is noticed, with a peak-to-peak close to 10%, a spring (between April and May) maximum and an autumn minimum (September for GCMS and November for FTIR). The trend deduced from the GCMS data is also in good agreement with the deduced stable period from 2008 onwards.

Please cite this article as: Lejeune B, et al. Optimized approach to retrieve information on atmospheric carbonyl sulfide (OCS) above the Jungfraujoch station and change in its abundance since 1995. J Quant Spectrosc Radiat Transfer (2016), http://dx.doi.org/10.1016/j.jqsrt.2016.06.001

Our FTIR stratospheric component shows a more constant trend of $(+0.20 \pm 0.06)$ % yr^{-1} (2σ) for the 1995–2015 period, very similar to those noticed in the Southern Hemisphere stratosphere by [28], and confirmed by solar occultation measurements recorded in the 41.5° to 51.5° northern latitude between 2004 and 2012 with the ACE-FTS instrument on-board SCISAT. This slight increase in the stratospheric trend seems too weak to support the increasing rate detected in the stratospheric aerosol backscatter.

The lack of modulation in the stratospheric partial column time series demonstrate that the decreasing/increasing trends detected for the 1995–2002 and 2002–2008 periods are clearly driven by tropospheric processes. A recent OCS anthropogenic inventory [33] and the last report of SO_2 emissions [69] provide evidence supporting a close relationship between the OCS signal recorded above JFJ and the anthropogenic sulfur emissions.

A sole time series does not suffice for identifying the causes of the non-monotonic long-term evolution of OCS with time. More datasets will be needed with a larger spatially and temporal distribution to improve our knowledge of OCS processes, together with targeted model studies that account for changes in the large-scale circulation (e.g., [72]) and OCS transport [28] as well as simulations with a chemical transport model like GEOS-Chem (e.g., [5,12]) focused on the vegetation uptake. It will be mandatory to evaluate the impact of the anthropogenic emissions of sulfur on the long-term trend of OCS.

We hope that the strategy described in this paper will encourage other studies in the framework of the NDACC network. Our strategy has been supplied to other partners [12,28]. Some adaptations might be necessary, to match site characteristics (e.g., humidity, altitude), but we are confident that the strategy described here constitutes a solid basis for future investigations.

Acknowledgments

The University of Liège involvement was primarily supported by BELSPO (Belgian Federal Science Policy Office, Brussels) through the ACROSAT project and by the GAW-CH program of MeteoSwiss. We are also grateful to the Fédération Wallonie-Bruxelles and the F.R.S. – FNRS for supporting mission expenses and laboratory developments, respectively. Emmanuel Mahieu is a Research Associate with the F.R.S. – FNRS. We are grateful to the many Belgian colleagues who have performed the FTIR observations used here. The Atmospheric Chemistry Experiment (ACE), also known as SCISAT, is a Canadian-led mission supported primarily by the Canadian Space Agency. The ground-based GCMS measurements are conducted under the auspices of the HALCLIM project funded by the Swiss Federal Office for the Environment (FOEN). We thank the International Foundation High Altitude Research Stations Jungfraujoch and Gornergrat (HFSJG, Bern) for supporting the facilities needed to perform the FTIR and GCMS measurements.

Appendix A. Supporting information

Supplementary data associated with this article can be found in the online version at http://dx.doi.org/10.1016/j.jqsrt.2016.06.001.

References

[1] Carpenter LJ, Reimann S, Lead Authors, Burkholder JB, Clerbaux C, Hall BD, Hossaini R, Laube JC, Yvon-Lewis SA. Ozone-Depleting Substances (ODSs) and other gases of interest to the Montreal protocol.Chapter 1 in Scientific assessment of ozone depletion: 2014, Global ozone research and monitoring project – Report No. 55. Geneva, Switzerland: World Meteorological Organization; 2014.

[2] Montzka SA, Calvert P, Hall BD, Elkins JW, Conway TJ, Tans PP, Sweeney C. On the global distribution, seasonality, and budget of atmospheric carbonyl sulfide (COS) and some similarities to CO_2. J Geophys Res 2007;112(D9). http://dx.doi.org/10.1029/2006JD007665.

[3] Kettle AJ, Kuhn U, von Hobe M, Kesselmeier J, Andreae MO. Global budget of atmospheric carbonyl sulfide: Temporal and spatial variations of the dominant sources and sinks. ACH 25–1. J Geophys Res: Atmos 2002;107(D22). http://dx.doi.org/10.1029/2002JD002187.

[4] Crutzen PJ. The possible importance of CSO for the sulfate layer of the stratosphere. Geophys Res Lett 1976;3(2):73–6. http://dx.doi.org/10.1029/GL003i002p00073.

[5] Suntharalingam P, Kettle AJ, Montzka SM, Jacob DJ. Global 3-D model analysis of the seasonal cycle of atmospheric carbonyl sulfide: implications for terrestrial vegetation uptake. Geophys Res Lett 2008;35(19). http://dx.doi.org/10.1029/2008GL034332.

[6] Campbell JE, Carmichael GR, Chai T, Mena-Carrasco M, Tang Y, Blake DR, Blake NJ, Vay SA, Collatz GJ, Baker I, Berry JA, Montzka SA, Sweeney C, Schnoor JL, Stanier CO. Photosynthetic control of atmospheric carbonyl sulfide during the growing season. Science 2008;322(5904):1085–8. http://dx.doi.org/10.1126/science.1164015.

[7] Blonquist JM, Montzka SA, Munger JW, Yakir D, Desai AR, Dragoni D, Griffis TJ, Monson RK, Scott RL, Bowling DR. The potential of carbonyl sulfide as a proxy for gross primary production at flux tower sites. J Geophys Res 2011;116(G4). http://dx.doi.org/10.1029/2011JG001723.

[8] Berry J, Wolf A, Campbell JE, Baker I, Blake N, Blake D, Denning AS, Kawa SR, Montzka SA, Seibt U, Stimler K, Yakir D, Zhu Z. A coupled model of the global cycles of carbonyl sulfide and CO_2: a possible new window on the carbon cycle. J Geophys Res: Biogeosci 2013;118(2):842–52. http://dx.doi.org/10.1002/jgrg.20068.

[9] Commane R, Herndon SC, Zahniser MS, Lerner BM, McManus JB, Munger JW, Nelson DD, Wofsy SC. Carbonyl sulfide in the planetary boundary layer: coastal and continental influences. J Geophys Res: Atmos 2013;118(14):8001–9. http://dx.doi.org/10.1002/jgrd.50581.

[10] Launois T, Peylin P, Belviso S, Poulter B. A new model of the global biogeochemical cycle of carbonyl sulfide – Part 2: use of carbonyl sulfide to constrain gross primary productivity in current vegetation models. Atmos Chem Phys 2015;15(16):9285–312, http://dx.doi.org/10.5194/acp-15-9285-2015.

[11] Commane R, Meredith LK, Baker IT, Berry JA, Munger JW, Montzka SA, Templer PH, Juice SM, Zahniser MS, Wofsy SC. Seasonal fluxes of carbonyl sulfide in a midlatitude forest. Proc Natl Acad Sci 2015;112(46):14162–7. http://dx.doi.org/10.1073/pnas.1504131112.

[12] Wang Y, Deutscher NM, Palm M, Warneke T, Notholt J, Baker I, Berry J, Suntharalingam P, Jones N, Mahieu E, Lejeune B, Hannigan J, Conway S, Mendonca J, Strong K, Campbell JE, Wolf A, Kremser S. Towards understanding the variability in biospheric CO_2 fluxes: using FTIR spectrometry and a chemical transport model to investigate the sources and sinks of carbonyl sulfide and its link to CO_2. Atmos Chem Phys 2016;16(4):2123–38. http://dx.doi.org/10.5194/acp-16-2123-2016.

[13] Watts SF. The mass budgets of carbonyl sulfide, dimethyl sulfide, carbon disulfide and hydrogen sulfide. Atmos Environ 2000;34(5):761–79. http://dx.doi.org/10.1016/S1352-2310(99)00342-8.

[14] Glatthor N, Höpfner M, Baker IT, Berry J, Campbell JE, Kawa SR, Krysztofiak G, Leyser A, Sinnhuber B-M, Stiller GP, Stinecipher J, von Clarmann T. Tropical sources and sinks of carbonyl sulfide observed from space. Geophys Res Lett 2015;42(22):10,082–90, http://dx.doi.org/10.1002/2015GL066293.

[15] SPARC (Stratosphere-troposphere Processes And their Role in Climate). SPARC assessment of stratospheric aerosol properties. In: Thomason L and Peter Th (editors). World Climate Research Program Report 124, SPARC Report 4, WMO/TD- No. 1295. Verrières le Buisson: France; 2006. 346 p.

Please cite this article as: Lejeune B, et al. Optimized approach to retrieve information on atmospheric carbonyl sulfide (OCS) above the Jungfraujoch station and change in its abundance since 1995. J Quant Spectrosc Radiat Transfer (2016), http://dx.doi.org/10.1016/j.jqsrt.2016.06.001

[16] Junge CE, Chagnon CW, Manson JE. Stratospheric aerosols. J Meteorol 1961;18(1):81–108. http://dx.doi.org/10.1175/1520-0469(1961)018<0081:SA>2.0.CO;2.

[17] Chin M, Davis DD. A reanalysis of carbonyl sulfide as a source of stratospheric background sulfur aerosol. J Geophys Res 1995;100 (D5):8993. http://dx.doi.org/10.1029/95JD00275.

[18] Kjellström E. A three-dimensional global model study of carbonyl sulfide in the troposphere and the lower stratosphere. J Atmos Chem 1998;29(2):151–77. http://dx.doi.org/10.1023/A:1005976511096.

[19] Leung F-YT, Colussi AJ, Hoffmann MR, Toon GC. Isotopic fractionation of carbonyl sulfide in the atmosphere: implications for the source of background stratospheric sulfate aerosol. 112–1–112–114. Geophys Res Lett 2002;29(10). http://dx.doi.org/10.1029/2001GL013955.

[20] Myhre G, Berglen TF, Myhre CEL, Isaksen ISA. The radiative effect of the anthropogenic influence on the stratospheric sulfate aerosol layer. Tellus B 2004;56(3):294–9. http://dx.doi.org/10.1111/j.1600-0889.2004.00106.x.

[21] Hattori S, Danielache SO, Johnson MS, Schmidt JA, Kjaergaard HG, Toyoda S, Ueno Y, Yoshida N. Ultraviolet absorption cross sections of carbonyl sulfide isotopologues $OC^{32}S$, $OC^{33}S$, $OC^{34}S$ and $O^{13}CS$: isotopic fractionation in photolysis and atmospheric implications. Atmos Chem Phys 2011;11(19):10293–303. http://dx.doi.org/10.5194/acp-11-10293-2011.

[22] Brühl C, Lelieveld J, Crutzen PJ, Tost H. The role of carbonyl sulphide as a source of stratospheric sulphate aerosol and its impact on climate. Atmos Chem Phys 2012;12(3):1239–53. http://dx.doi.org/10.5194/acp-12-1239-2012.

[23] Schmidt JA, Johnson MS, Hattori S, Yoshida N, Nanbu S, Schinke R. OCS photolytic isotope effects from first principles: sulfur and carbon isotopes, temperature dependence and implications for the stratosphere. Atmos Chem Phys 2013;13(3):1511–20, http://dx.doi.org/10.5194/acp-13-1511-2013.

[24] Sheng J-X, Weisenstein DK, Luo B-P, Rozanov E, Stenke A, Anet J, Bingemer H, Peter T. Global atmospheric sulfur budget under volcanically quiescent conditions: aerosol-chemistry-climate model predictions and validation. J Geophys Res: Atmos 2015;120(1): 256–76. http://dx.doi.org/10.1002/2014JD021985.

[25] Rinsland CP, Goldman A, Mahieu E, Zander R, Notholt J, Jones NB, Griffith DWT, Stephen TM, Chiou LS. Ground-based infrared spectroscopic measurements of carbonyl sulfide: free tropospheric trends from a 24-year time series of solar absorption measurements. ACH 24–1. J Geophys Res: Atmos 2002;107(D22). http://dx.doi.org/10.1029/2002JD002522.

[26] Hofmann D, Barnes J, O'Neill M, Trudeau M, Neely R. Increase in background stratospheric aerosol observed with lidar at Mauna Loa Observatory and Boulder, Colorado. Geophys Res Lett 2009;36(15). http://dx.doi.org/10.1029/2009GL039008.

[27] Zander R, Mahieu E, Demoulin P, Duchatelet P, Servais C, Roland G, DelBouille L, De Mazière M, Rinsland CP. Evolution of a dozen non-CO_2 greenhouse gases above central Europe since the mid-1980s. Environ Sci 2005;2(2–3):295–303. http://dx.doi.org/10.1080/15693430500397152.

[28] Kremser S, Jones NB, Palm M, Lejeune B, Wang Y, Smale D, Deutscher NM. Positive trends in Southern Hemisphere carbonyl sulfide. Geophys Res Lett 2015;42(21):9473–80. http://dx.doi.org/10.1002/2015GL065879.

[29] Montzka SA, Reimann S, Coordinating Lead Authors, Engel A, Krüger K, O'Doherty S, Sturges WT, Lead Authors, Blake D, Dorf M, Fraser P, Froidevaux L, Jucks K, Kreher K, Kurylo MJ, Mellouki A, Miller J, Nielsen O-J, Orkin VL, Prinn RG, Rhew R, Santee ML, Stohl A, Verdonik D. Ozone-Depleting Substances (ODSs) and related chemicals, Chapter 1 in Scientific assessment of ozone depletion: 2010.Global ozone research and monitoring project – Report No. 52. Geneva, Switzerland: World Meteorological Organization; 2011.

[30] Turco RP, Whitten RC, Toon OB, Pollack JB, Hamill P. OCS, stratospheric aerosols and climate. Nature 1980;283(5744): 283–5. http://dx.doi.org/10.1038/283283a0.

[31] Khalil MAK, Rasmussen RA. Global sources, lifetimes and mass balances of carbonyl sulfide (OCS) and carbon disulfide (CS_2) in the earth's atmosphere. Atmos Environ (1967) 1984;18(9): 1805–13. http://dx.doi.org/10.1016/0004-6981(84)90356-1.

[32] Blake NJ, Streets DG, Woo J-H, Simpson IJ, Green J, Meinardi S, Kita K, Atlas E, Fuelberg HE, Sachse G, Avery MA, Vay SA, Talbot RW, Dibb JE, Bandy AR, Thornton DC, Rowland FS, Blake DR. Carbonyl sulfide and carbon disulfide: large-scale distributions over the western Pacific and emissions from Asia during TRACE-P. J Geophys Res: Atmos 2004;109(D15). http://dx.doi.org/10.1029/2003JD004259.

[33] Campbell JE, Whelan ME, Seibt U, Smith SJ, Berry JA, Hilton TW. Atmospheric carbonyl sulfide sources from anthropogenic activity: implications for carbon cycle constraints. Geophys Res Lett 2015;42 (8):3004–10. http://dx.doi.org/10.1002/2015GL063445.

[34] Montzka SA, Aydin M, Battle M, Butler JH, Saltzman ES, Hall BD, Clarke AD, Mondeel D, Elkins JW. A 350-year atmospheric history for carbonyl sulfide inferred from Antarctic firn air and air trapped in ice. J Geophys Res: Atmos 2004;109(D22). http://dx.doi.org/10.1029/2004JD004686.

[35] Aydin M, Fudge TJ, Verhulst KR, Nicewonger MR, Waddington ED, Saltzman ES. Carbonyl sulfide hydrolysis in Antarctic ice cores and an atmospheric history for the last 8000 years. J Geophys Res: Atmos 2014;119(13):8500–14. http://dx.doi.org/10.1002/2014JD021618.

[36] Zander R, Mahieu E, Demoulin P, Duchatelet P, Roland G, Servais C, Mazière MD, Reimann S, Rinsland CP. Our changing atmosphere: evidence based on long-term infrared solar observations at the Jungfraujoch since 1950. Sci Total Environ 2008;391(2–3): 184–95. http://dx.doi.org/10.1016/j.scitotenv.2007.10.018.

[37] Rodgers CD. Retrieval of atmospheric temperature and composition from remote measurements of thermal radiation. Rev Geophys 1976;14(4):609. http://dx.doi.org/10.1029/RG014i004p00609.

[38] Rinsland CP, Jones NB, Connor BJ, Logan JA, Pougatchev NS, Goldman A, Murcray FJ, Stephen TM, Pine AS, Zander R, Mahieu E, Demoulin P. Northern and southern hemisphere ground-based infrared spectroscopic measurements of tropospheric carbon monoxide and ethane. J Geophys Res 1998;103(D21):28197. http://dx.doi.org/10.1029/98JD02515.

[39] Hase F, Hannigan JW, Coffey MT, Goldman A, Höpfner M, Jones NB, Rinsland CP, Wood SW. Intercomparison of retrieval codes used for the analysis of high-resolution, ground-based FTIR measurements. J Quant Spectrosc Radiat Transf 2004;87(1): 25–52. http://dx.doi.org/10.1016/j.jqsrt.2003.12.008.

[40] Duchatelet P, Demoulin P, Hase F, Ruhnke R, Feng W, Chipperfield MP, Bernath PF, Boone CD, Walker KA, Mahieu E. Hydrogen fluoride total and partial column time series above the Jungfraujoch from long-term FTIR measurements: impact of the line-shape model, characterization of the error budget and seasonal cycle, and comparison with satellite and model data. J Geophys Res 2010;115(D22). http://dx.doi.org/10.1029/2010JD014677.

[41] Rothman LS, Gordon IE, Babikov Y, Barbe A, Chris Benner D, Bernath PF, Birk M, Bizzocchi L, Boudon V, Brown LR, Campargue A, Chance K, Cohen EA, Coudert LH, Devi VM, Drouin BJ, Fayt A, Flaud J-M, Gamache RR, Harrison JJ, Hartmann J-M, Hill C, Hodges JT, Jacquemart D, Jolly A, Lamouroux J, Le Roy RJ, Li G, Long DA, Lyulin OM, Mackie CJ, Massie ST, Mikhailenko S, Müller HSP, Naumenko OV, Nikitin AV, Orphal J, Perevalov V, Perrin A, Polovtseva ER, Richard C, Smith MAH, Starikova E, Sung K, Tashkun S, Tennyson J, Toon GC, Tyuterev VG, Wagner G. The HITRAN2012 molecular spectroscopic database. J Quant Spectrosc Radiat Transf 2013;130:4–50, http://dx.doi.org/10.1016/j.jqsrt.2013.07.002.

[42] Rothman LS, Gordon IE, Barbe A, Benner DC, Bernath PF, Birk M, Boudon V, Brown LR, Campargue A, Champion J-P, Chance K, Coudert LH, Dana V, Devi VM, Fally S, Flaud J-M, Gamache RR, Goldman A, Jacquemart D, Kleiner I, Lacome N, Lafferty WJ, Mandin J-Y, Massie ST, Mikhailenko SN, Miller CE, Moazzen-Ahmadi N, Naumenko OV, Nikitin AV, Orphal J, Perevalov VI, Perrin A, Predoi-Cross A, Rinsland CP, Rotger M, Šimečková M, Smith MAH, Sung K, Tashkun SA, Tennyson J, Toth RA, Vandaele AC, Vander Auwera J. The HITRAN 2008 molecular spectroscopic database. J Quant Spectrosc Radiat Transf 2009;110(9–10):533–72. http://dx.doi.org/10.1016/j.jqsrt.2009.02.013.

[43] Rothman LS, Jacquemart D, Barbe A, Chris Benner D, Birk M, Brown LR, Carleer MR, Chackerian C, Chance K, Coudert LH, Dana V, Devi VM, Flaud J-M, Gamache RR, Goldman A, Hartmann J-M, Jucks KW, Maki AG, Mandin J-Y, Massie ST, Orphal J, Perrin A, Rinsland CP, Smith MAH, Tennyson J, Tolchenov RN, Toth RA, Vander Auwera J, Varanasi P, Wagner G. The HITRAN 2004 molecular spectroscopic database. J Quant Spectrosc Radiat Transf 2005;96(2): 139–204. http://dx.doi.org/10.1016/j.jqsrt.2004.10.008.

[44] Bernath PF, McElroy CT, Abrams MC, Boone CD, Butler M, Camy-Peyret C, Carleer M, Clerbaux C, Coheur P-F, Colin R, DeCola P, De Mazière M, Drummond JR, Dufour D, Evans WFJ, Fast H, Fussen D, Gilbert K, Jennings DE, Llewellyn EJ, Lowe RP, Mahieu E, McConnell JC, McHugh M, McLeod SD, Michaud R, Midwinter C, Nassar R, Nichitiu F, Nowlan C, Rinsland CP, Rochon YJ, Rowlands N, Semeniuk K, Simon P, Skelton R, Sloan JJ, Soucy M-A, Strong K, Tremblay P, Turnbull D, Walker KA, Walkty I, Wardle DA, Wehrle V, Zander R, Zou J. Atmospheric Chemistry Experiment (ACE): mission overview. Geophys Res Lett 2005;32(15). http://dx.doi.org/10.1029/2005GL022386.

[45] Bernath PF. The atmospheric chemistry experiment (ACE); 2016 (this issue).

Please cite this article as: Lejeune B, et al. Optimized approach to retrieve information on atmospheric carbonyl sulfide (OCS) above the Jungfraujoch station and change in its abundance since 1995. J Quant Spectrosc Radiat Transfer (2016), http://dx.doi.org/10.1016/j.jqsrt.2016.06.001

[46] Chang L, Palo S, Hagan M, Richter J, Garcia R, Riggin D, Fritts D. Structure of the migrating diurnal tide in the Whole Atmosphere Community Climate Model (WACCM). Adv Space Res 2008;41(9): 1398–407. http://dx.doi.org/10.1016/j.asr.2007.03.035.

[47] Sussmann R, Borsdorff T, Rettinger M, Camy-Peyret C, Demoulin P, Duchatelet P, Mahieu E, Servais C. Technical Note: harmonized retrieval of column-integrated atmospheric water vapor from the FTIR network – first examples for long-term records and station trends. Atmos Chem Phys 2009;9(22):8987–99, http://dx.doi.org/10.5194/acp-9-8987-2009.

[48] Dils B, Cui J, Henne S, Mahieu E, Steinbacher M, De Mazière M. 1997–2007 CO trend at the high alpine site Jungfraujoch: a comparison between NDIR surface in situ and FTIR remote sensing observations. Atmos Chem Phys 2011;11(13):6735–48. http://dx.doi.org/10.5194/acp-11-6735-2011.

[49] Barret B, De Mazière M, Demoulin P. Retrieval and characterization of ozone profiles from solar infrared spectra at the Jungfraujoch. ACH 19–1–ACH 19–15. J Geophys Res: Atmos 2002;107(D24). http://dx.doi.org/10.1029/2001JD001298.

[50] Hase F, Demoulin P, Sauval AJ, Toon GC, Bernath PF, Goldman A, Hannigan JW, Rinsland CP. An empirical line-by-line model for the infrared solar transmittance spectrum from 700 to 5000 cm^{-1}. J Quant Spectrosc Radiat Transf 2006;102(3):450–63. http://dx.doi.org/10.1016/j.jqsrt.2006.02.026.

[51] Vigouroux C, Blumenstock T, Coffey M, Errera Q, García O, Jones NB, Hannigan JW, Hase F, Liley B, Mahieu E, Mellqvist J, Notholt J, Palm M, Persson G, Schneider M, Servais C, Smale D, Thölix L, De Mazière M. Trends of ozone total columns and vertical distribution from FTIR observations at eight NDACC stations around the globe. Atmos Chem Phys 2015;15(6):2915–33. http://dx.doi.org/10.5194/acp-15-2915-2015.

[52] Rinsland CP, Zander R, Mahieu E, Demoulin P, Goldman A, Ehhalt DH, Rudolph J. Ground-based infrared measurements of carbonyl sulfide total column abundances: long-term trends and variability. J Geophys Res 1992;97(D5):5995. http://dx.doi.org/10.1029/92JD00040.

[53] Krysztofiak G, Té YV, Catoire V, Berthet G, Toon GC, Jégou F, Jeseck P, Robert C. Carbonyl sulphide (OCS) variability with latitude in the atmosphere. Atmos-Ocean 2015;53(1):89–101, http://dx.doi.org/10.1080/07055900.2013.876609.

[54] Rodgers CD. Characterization and error analysis of profiles retrieved from remote sounding measurements. J Geophys Res 1990;95(D5): 5587. http://dx.doi.org/10.1029/JD095iD05p05587.

[55] Griffith DWT, Jones NB, Matthews WA. Interhemispheric ratio and annual cycle of carbonyl sulfide (OCS) total column from ground-based solar FTIR spectra. J Geophys Res: Atmos 1998;103(D7): 8447–54. http://dx.doi.org/10.1029/97JD03462.

[56] Barthlott S, Schneider M, Hase F, Wiegele A, Christner E, González Y, Blumenstock T, Dohe S, García OE, Sepúlveda E, Strong K, Mendonca J, Weaver D, Palm M, Deutscher NM, Warneke T, Notholt J, Lejeune B, Mahieu E, Jones N, Griffith DWT, Velazco VA, Smale D, Robinson J, Kivi R, Heikkinen P, Raffalski U. Using XCO_2 retrievals for assessing the long-term consistency of NDACC/FTIR data sets. Atmos Meas Tech 2015;8(3):1555–73. http://dx.doi.org/10.5194/amt-8-1555-2015.

[57] Franco B, Hendrick F, Van Roozendael M, Müller J-F, Stavrakou T, Marais EA, Bovy B, Bader W, Fayt C, Hermans C, Lejeune B, Pinardi G, Servais C, Mahieu E. Retrievals of formaldehyde from ground-based FTIR and MAX-DOAS observations at the Jungfraujoch station and comparisons with GEOS-Chem and IMAGES model simulations. Atmos Meas Tech 2015;8(4):1733–56. http://dx.doi.org/10.5194/amt-8-1733-2015.

[58] Rodgers CD. Inverse methods for atmospheric sounding: theory and practice. Series on atmospheric oceanic and planetary physics, vol. 2. Singapore: World Scientific Publishing Co.; 2000.

[59] Irion FW, Gunson MR, Toon GC, Chang AY, Eldering A, Mahieu E, Manney GL, Michelsen HA, Moyer EJ, Newchurch MJ, Osterman GB, Rinsland CP, Salawitch RJ, Sen B, Yung YL, Zander R. Atmospheric Trace Molecule Spectroscopy (ATMOS) experiment version 3 data retrievals. Appl Opt 2002;41(33):6968. http://dx.doi.org/10.1364/AO.41.006968.

[60] Régalia-Jarlot L, Hamdouni A, Thomas X, Von der Heyden P, Barbe A. Line intensities of the: ν_3, $4\nu_2$, $\nu_1+\nu_3$, $3\nu_1$ and $2\nu_1+2\nu_2$ bands of $^{16}O^{12}C^{32}S$ molecule. J Quant Spectrosc Radiat Transf 2002;74(4): 455–70. http://dx.doi.org/10.1016/S0022-4073(01)00267-9.

[61] Vander Auwera J, Fayt A. Absolute line intensities for carbonyl sulfide from 827 to 2939 cm^{-1}. J Mol Struct 2006;780–781: 134–41. http://dx.doi.org/10.1016/j.molstruc.2005.04.052.

[62] Miller BR, Weiss RF, Salameh PK, Tanhua T, Greally BR, Mühle J, Simmonds PG. Medusa: a sample preconcentration and GC/MS detector system for in situ measurements of atmospheric trace halocarbons, hydrocarbons, and sulfur compounds. Anal Chem 2008;80(5):1536–45. http://dx.doi.org/10.1021/ac702084k.

[63] Vollmer MK, Miller BR, Rigby M, Reimann S, Mühle J, Krummel PB, O'Doherty S, Kim J, Rhee TS, Weiss RF, Fraser PJ, Simmonds PG, Salameh PK, Harth CM, Wang RHJ, Steele LP, Young D, Lunder CR, Hermansen O, Ivy D, Arnold T, Schmidbauer N, Kim K-R, Greally BR, Hill M, Leist M, Wenger A, Prinn RG. Atmospheric histories and global emissions of the anthropogenic hydrofluorocarbons HFC-365mfc, HFC-245fa, HFC-227ea, and HFC-236fa. J Geophys Res 2011;116(D8). http://dx.doi.org/10.1029/2010JD015309.

[64] Gardiner T, Forbes A, de Mazière M, Vigouroux C, Mahieu E, Demoulin P, Velazco V, Notholt J, Blumenstock T, Hase F, Kramer I, Sussmann R, Stremme W, Mellqvist J, Strandberg A, Ellingsen K, Gauss M. Trend analysis of greenhouse gases over Europe measured by a network of ground-based remote FTIR instruments. Atmos Chem Phys 2008;8(22):6719–27. http://dx.doi.org/10.5194/acp-8-6719-2008.

[65] Mahieu E, Zander R, Toon GC, Vollmer MK, Reimann S, Mühle J, Bader W, Bovy B, Lejeune B, Servais C, Demoulin P, Roland G, Bernath PF, Boone CD, Walker KA, Duchatelet P. Spectrometric monitoring of atmospheric carbon tetrafluoride (CF_4) above the Jungfraujoch station since 1989: evidence of continued increase but at a slowing rate. Atmos Meas Tech 2014;7(1):333–44, http://dx.doi.org/10.5194/amt-7-333-2014.

[66] Barkley MP, Palmer PI, Boone CD, Bernath PF, Suntharalingam P. Global distributions of carbonyl sulfide in the upper troposphere and stratosphere. Geophys Res Lett 2008;35: L14810. http://dx.doi.org/10.1029/2008GL034270.

[67] Boone CD, Walker KA, Bernath PF. Version 3 retrievals for the atmospheric chemistry experiment fourier transform spectrometer (ACE-FTS). In: Bernath PF, Deepak A, editors. The atmospheric chemistry experiment ACE at 10: a solar occultation anthology. USA: Publishing, Hampton, Virginia; 2013. p. 103–27.

[68] Sturges WT, Penkett SA, Barnola J-M, Chappellaz J, Atlas E, Stroud V. A long-term record of carbonyl sulfide (COS) in two hemispheres from firn air measurements. Geophys Res Lett 2001;28(21): 4095–8. http://dx.doi.org/10.1029/2001GL013958.

[69] Klimont Z, Smith SJ, Cofala J. The last decade of global anthropogenic sulfur dioxide: 2000–2011 emissions. Environ Res Lett 2013;8(1): 014003. http://dx.doi.org/10.1088/1748-9326/8/1/014003.

[70] Coffey MT, Hannigan JW. The temporal trend of stratospheric carbonyl sulfide. J Atmos Chem 2010;67(1):61–70. http://dx.doi.org/10.1007/s10874-011-9203-4.

[71] Rinsland CP, Chiou L, Mahieu E, Zander R, Boone CD, Bernath PF. Measurements of long-term changes in atmospheric OCS (carbonyl sulfide) from infrared solar observations. J Quant Spectrosc Radiat Transf 2008;109(16):2679–86. http://dx.doi.org/10.1016/j.jqsrt.2008.07.008.

[72] Mahieu E, Chipperfield MP, Notholt J, Reddmann T, Anderson J, Bernath PF, Blumenstock T, Coffey MT, Dhomse SS, Feng W, Franco B, Froidevaux L, Griffith DWT, Hannigan JW, Hase F, Hossaini R, Jones NB, Morino I, Murata I, Nakajima H, Palm M, Paton-Walsh C, Russell JM, Schneider M, Servais C, Smale D, Walker KA. Recent northern hemisphere stratospheric HCl increase due to atmospheric circulation changes. Nature 2014;515(7525):104–7, http://dx.doi.org/10.1038/nature13857.

Please cite this article as: Lejeune B, et al. Optimized approach to retrieve information on atmospheric carbonyl sulfide (OCS) above the Jungfraujoch station and change in its abundance since 1995. J Quant Spectrosc Radiat Transfer (2016), http://dx.doi.org/10.1016/j.jqsrt.2016.06.001